Intradomain Distances in the Regulatory Domain of the Myosin Head in Prepower and Postpower Stroke States: Fluorescence Energy Transfer†

Thomas Palm,‡,§ Ken Sale,‡,§ Louise Brown,|| Huichun Li,‡ Brett Hambly,|| and Peter G. Fajer*,‡

The National High Magnetic Field Laboratory, Institute of Molecular Biophysics, and Department of Biological Science, Florida State University, Tallahassee, Florida 32306, and Department of Pathology, University of Sydney NSW 2006, Australia

Received May 20, 1999; Revised Manuscript Received July 27, 1999

ABSTRACT: The relative movement of the catalytic and regulatory domains of the myosin head (S1) is likely to be the force generating conformational change in the energy transduction of muscle [Rayment, I., Holden, H. M., Whittaker, M., Yohn, C. B., Lorenz, M., Holmes, K. C., and Milligan, R. A. (1993) *Science 261*, 58−65]. To test this model we have measured, using frequency-modulated FRET, three distances between the catalytic domain and regulatory domains and within the regulatory domain of myosin. The donor/acceptor pairs included MHC cys707 and ELC cys177; ELC cys177 and RLC cys154; and ELC cys177 and gizzard RLC cys108. The IAEDANS (donor) or acceptor (DABMI or IAF) labeled light chains (ELC and RLC) were exchanged into monomeric myosin and the distances were measured in the putative prepower stroke states (in the presence of MgATP or ADP/AlF_4^-) and the postpower stroke states (ADP and the absence of nucleotides). For each of the three distances, the donor/acceptor pairs were reversed to minimize uncertainty in the distance measured, arising from probe orientational factors. The distances obtained from FRET were in close agreement with the distances in the crystal structure. Importantly, none of the measured distances varied by more than 2 Å, putting a strong constraint on the extent of conformational changes within S1. The maximum axial movement of the distal part of myosin head was modeled using FRET distance changes within the myosin head reported here and previously. These models revealed an upper bound of 85 Å for a swing of the regulatory domain with respect to the catalytic domain during the power stroke. Additionally, an upper bound of 22 Å could be contributed to the power stroke by a reorientation of RLC with respect to the ELC during the power stroke.

The myosin head (subfragment-1, S1)[1] consists of two parts: a heavy-chain catalytic domain that binds actin and the nucleotide substrate, and a regulatory domain consisting of two calmodulin-like light chains enclosing a long heavy chain α-helix (*2*) originating in the catalytic domain. The essential light chain (ELC) is proximal to the catalytic domain, while the regulatory light chain (RLC) is distal and provides a link to the myosin filament. Several lines of evidence have led to a model of muscle contraction where mechanical torque is produced by a conformational change in the catalytic domain of the myosin head, followed by rotation of the regulatory domain, which acts as a mechanical lever (*3*, *4*). Since the myosin head is an elongated molecule, such a rotation of the regulatory domain is likely to result in a change of shape. Evidence for nucleotide-induced conformational changes in S1 has been provided by transient electrical birefringence and by neutron and X-ray scattering, where the binding of MgATP and nucleotide analogues (*3*, *5*, *6*) appear to make S1 more compact. Solution of the atomic structure of S1 in intermediate states has revealed a prepower stroke state in which S1 exhibits a compact structure, forming an angle of approximately 70° between the catalytic and regulatory domains (*7*, *8*), compared to the more extended structure of S1 in the presumed postpower stroke state (*1*). However, no crystal structure of the two states has been obtained from a full-length myosin head and from the same myosin isoform. At least in one case, M.ADP.BeF_x, different shapes have been observed in constructs with varying length of the regulatory domain and between skeletal and smooth muscle isoforms (*1*, *8*).

Conformational changes are not limited to the transition between pre- and postpower stroke states. Electron microscopic reconstructions of smooth and nonmuscle S1 bound to actin filaments reveal a 30° rotation of the regulatory domain with respect to the catalytic domain upon MgADP binding (*9*, *10*); both states are believed to be postpower

† Research sponsored by National Science Foundation NSF-IBN-9808708, NHMFL In-House grant, American Heart Association GIA-9950424N, NIH HL26043, and the NHMRC of Australia. K.S. is a NSF Research Training Grant Fellow, DBI-9602233.

* To whom correspondence should be addressed. E-mail: fajer@magnet.fsu.edu.

‡ Institute of Molecular Biophysics and Florida State University.

§ Both authors contributed to the project in equal amounts.

|| University of Sydney.

[1] Abbreviations: ADP, adenosine 5′-diphosphate; AEDANS, 5-(acetamidoethyl)aminonaphthalene-1-sulfonic acid; AF, 5-(acetamido)fluorescein; ATP, adenosine 5′ triphosphate; DABMI, 4-dimethylaminophenylazophenyl-4′-maleimide; DMF, *N*,*N*′-dimethyl formamide; DTT, dithiothreitol; EDTA, ethylenediaminetetraacetic acid aminoethyl ether; ELC, skeletal essential light chain, A1 isoform; gRLC, gizzard smooth muscle RLC; IAEDANS, 5-(iodoacetamidoethyl)aminonaphthalene-1-sulfonic acid; IAF, 5-(iodoacetamido)fluorescein; LC3, skeletal light chain 3; Mops, 3-(N-morpholino)propanesulfonic acid; MHC, skeletal myosin heavy chain; OD, optical density; RLC, skeletal regulatory light chain; RLC-C125R, recombinant regulatory light chain with only one cysteine at position 154; S1, myosin subfragment 1; Tris, tris-(hydroxymethyl)-aminomethane.

10.1021/bi991164z CCC: $18.00
Published on Web 09/14/1999

stroke states. This change was confirmed by EPR to exist in smooth muscle fibers (*4*). The extension of solution or crystal studies to muscle fibers is of considerable importance. If these conformational changes are driving force generation, then they have to be observed within the constraints of the myofibrillar lattice. Such efforts are encouraging, and complementary EPR, fluorescence, and phosphorescence spectroscopic studies have demonstrated a small ordered fraction of catalytic domain during steady-state force generation in fibers (*11*), but in the regulatory domain, either disorder (*12*) or the formation of new angular distributions (*13*) has been observed.

Implicit in any of the models postulating rotation of the regulatory domain is the presence of a point of flexibility, a hinge, located within the myosin head region. Recently, saturation transfer EPR (ST-EPR) measurements have shown that a flexible hinge exists between the catalytic domain and the ELC of the regulatory domain. The hinge was observed in the absence of actin and nucleotide (*14*) and is presumed to stiffen during force generation.

Using FRET several attempts have been made to detect distance changes within the myosin head in response to nucleotide analogue binding following the pioneering efforts of Morales and collaborators reviewed in refs *15* and *16*. The results have been generally inconclusive: Marsh and Lowey (*17*), Smyczynski and Kasprzak (*18*), Burmeister Getz et al. (*19*), and Xu and Root (*20*) did not detect any statistically significant change in the distance between sites in the catalytic domain and in the regulatory domain in response to the binding of nucleotide analogues and/or F-actin. However, the recent study of Selvin and collaborators reports on a significant compaction of the S1 structure in the prepower stroke state (*21*). The latter study measured a long cord distance from the catalytic domain to a distal portion of the regulatory domain. Clearly, the putative hinge could lie at any point spanned by this cord. We aim here to subdivide that cord distance measurement by determining shorter distances between the catalytic domain and the proximal part of the regulatory domain, as well as the intradomain distance between the ELC and RLC. The primary finding of our study is that there is no significant distance change between the ELC and RLC in response to nucleotide binding, thus excluding flexibility within the regulatory domain and pointing to the location of the hinge being part of the catalytic domain.

MATERIALS AND METHODS

Myosin was prepared using the method described by Eads et al. (*22*) and stored at −20 °C in 50% v/v glycerol, 0.5 M KCl, 0.5 mM EDTA, 0.5 mM DTT, 20 mM Mops, pH 7.0, at a concentration of 12 mg/mL. Mixed skeletal light chains were isolated from purified myosin using the guanidine-HCl method published by Wagner (*23*). The light chains were separated on a Cibacron Blue 3GA column (Sigma, St. Louis, MI) following the method of Toste and Cooke (*24*) and stored at −20 °C in 0.2 M KCl, 1 mM DTT, and 20 mM Tris, pH 7.5, at concentrations of 5 mg/mL (ELC, A1 isoform) and 1 mg/mL (RLC), respectively. Recombinant RLC-C125R, where cys125 was replaced by an arginine, leaving only one cysteine residue at position 154, was prepared as described by Boey et al. (*25*) and stored at −20 °C at a concentration of 1 mg/mL in 2 M urea, 0.5 mM $MgCl_2$, 100 mM NaCl, and 25 mM Tris, pH 7.5. RLC from chicken gizzard (gRLC) was prepared by the method of Grand and Perry (*26*) and stored at 3−4 mg/mL in 30 mM KCl and 20 mM Tris, pH 7.5, at −20 °C.

Labeling. (1) Catalytic Domain. Myosin heavy chain (MHC) cys707 (SH1) of the skeletal myosin head was labeled by adding an equimolar ratio of IAEDANS or DABMI from a 5 mM DMF stock solution to a solution of myosin (5−10 mg/mL) in 0.6 M KCl and 50 mM Tris, pH 7.5, as described by Marsh and Lowey (*17*). The mixture was allowed to react for 15 h at 4 °C. To separate labeled myosin from unreacted label, myosin was precipitated twice by diluting the mixture 25-fold with 2 mM EDTA and 10 mM Mops, pH 7.0, followed by sedimentation for 20 min at 10000*g*. The pellet was redissolved in 0.6 M KCl, 1 mM $MgCl_2$, and 50 mM Tris, pH 7.9.

(2) Regulatory Domain. Prior to labeling, skeletal ELC and recombinant RLC-C125R were incubated for 2 h at 22 °C in 6 M urea, 10 mM DTT, 50 mM KCl, and 50 mM Tris, pH 8.0. After dialysis against two changes of labeling buffer (6 M urea, 50 mM KCl, and 50 mM Tris, pH 8.0), the concentration of LC was adjusted to 3−6 mg/mL (ELC) or 1 mg/mL (RLC−C125R), and a 5-fold excess of IAEDANS, DABMI, or IAF was added from a stock solution (50 mM in DMF). The mixture was allowed to react for 5 h at 22 °C before reaction was stopped by adding 10 mM DTT and unreacted label was removed by exhaustive dialysis against labeling buffer. ELC was dialyzed into 300 mM KCl, 2 mM EDTA, and 100 mM Mops, pH 7.0, and RLC-C125R was dialyzed into 500 mM NaCl, 2 mM EDTA, and 40 mM Tris, pH 8.0.

Gizzard RLC^{108} was labeled as described by Kekic et al. (*27*). To ensure complete reduction of all sulfhydryl groups, the $gRLC^{108}$ was incubated for 2 h at 22 °C in 6 M guanidine HCl, 10 mM DTT, and 100 mM Tris, pH 8.0. After dialyzing into labeling buffer (100 mM NaCl, 2 mM EDTA, and 20 mM Mops, pH 7.0), the concentration of $gRLC^{108}$ was adjusted to 3 mg/mL, a 5-fold excess of IAEDANS or IAF was added from a 50 mM DMF-stock solution and the mixture was allowed to react for 1 h at 4 °C. The reaction was terminated by adding a 100-fold excess of DTT over label. Unreacted label was removed immediately by chromatography on Sephadex G-25 and dialysis into 500 mM NaCl, 2 mM EDTA, and 40 mM Tris, pH 8.0.

Labeling ratios were calculated by determining the protein concentration with the BCA protein assay (Pierce, Rockford, IL) and using the following extinction coefficients for the following labels: AEDANS, $\epsilon_{337} = 6.100\ mol^{-1}\ cm^{-1}$; AF, $\epsilon_{495} = 54.700\ mol^{-1}\ cm^{-1}$ (pH 7), $\epsilon_{495} = 99.600\ mol^{-1}\ cm^{-1}$ (pH 7.9); DABMI, $\epsilon_{460} = 24.800\ mol^{-1}\ cm^{-1}$.

Exchange of Light Chains. (1) Essential Light Chain. ELC was exchanged onto myosin by incubating a 10-fold excess of labeled or unlabeled ELC (1.3 mg/mL) over myosin (1.6 mg/mL) in 4.7 M NH_4Cl, 1 mM DTT, 5 mM ATP, 300 mM KCl, 2 mM EDTA, and 100 mM Mops, pH 7.0, for 30 min at 0 °C. The exchanged myosin was precipitated by dialysis into 40 mM KCl, 1 mM NaN_3, and 10 mM Mops, pH 7.0 for 2 h and sedimented for 20 min at 10000*g*. To remove any residual ELC, the myosin was redissolved in high ionic strength buffer (0.6 M KCl and 10 mM Tris, pH 7.0), precipitated for 20 min by a 25-fold dilution in 2 mM EDTA

and 10 mM Mops, pH 7.0, and sedimented for 20 min at 10000*g*. The myosin pellet was dissolved in either 500 mM NaCl, 2 mM EDTA, and 40 mM Tris, pH 8.0, for subsequent exchange of RLC or in fluorescence buffer (0.6 M KCl, 1 mM $MgCl_2$, 50 mM Tris, pH 7.9) for fluorescence measurements.

(2) Regulatory Light Chain. RLC-C125R and gRLC were exchanged onto myosin by incubating a 10−20-fold excess of RLC (0.5 mg/mL) over myosin (4 mg/mL) in 500 mM NaCl, 5 mM ATP, 2 mM DTT, 2 mM EDTA, and 40 mM Tris, pH 8.0, for 10 min at 38 °C. The exchange was stopped by addition of 10 mM $MgCl_2$ and cooling to 0 °C. Myosin was precipitated by dialysis against 1 mM $MgCl_2$ and 10 mM Mops, pH 7.0, and collected by centrifugation for 10 min at 10000*g*. Any residual light chains were removed by dissolving myosin in high ionic strength buffer and subsequent precipitation as described above. The myosin pellet was dissolved in fluorescence buffer.

ATPases. ATPase activity was assayed at 25 °C in 30 mM KCl, 3 mM $CaCl_2$, 1 mM $MgCl_2$, and 20 mM Mops, pH 7.0, as described by Wikman-Coffelt et al. (*28*). The reaction was initiated by adding 1 mM MgATP. Aliquots were taken at 2, 4, 6, and 8 min and the release of inorganic phosphate was determined by the method of Lanzetta et al. (*29*). Although the modification of the light chains has little (ELC) or no (RLC) effect on the MgATPases, the harsh conditions of the light change exchange sometimes affect myosin activity. Samples with more than 50% loss of activity were not used in the support of conclusions.

Fluorescence Measurements. Quantum yields were determined on a SPEX Fluoromax (SPEX, Edison, NJ) as described by Marsh and Lowey (*17*) using quinine bisulfate [quantum efficiency 0.7 in 0.1 N H_2SO_4 (*30*)] as a reference. Fluorescence lifetime data of AEDANS were collected with a SPEX Fluorolog τ2 (SPEX, Edison, NJ). Measurements were carried out at label concentrations of 1−3 μM in 0.6 M KCl, 1 mM $MgCl_2$, and 50 mM Tris, pH 7.9 (rigor solution). Other conditions were rigor solution plus 2 mM MgATP (ATP), rigor solution plus 0.2 mM ADP (ADP) and ADP solution plus 0.2 mM $AlCl_3$, and 5 mM NaF (*31*). The samples were excited with 20 mW (3 μM label) to 50 mW (1 μM label) UV light from an Innova 90 argon ion laser (Coherent, Santa Clara, CA) containing 334.0, 351.1, and 363.8 nm lines. Fluorescence emission was collected at 460 ± 15 nm when AF was the acceptor or at 485 ± 15 nm when DABMI was the acceptor. To minimize the inner filter effect, semi-microcuvettes were used and the OD at the emission wavelength of the solution was kept below 0.02.

Fluorescence Resonance Energy Transfer Analysis. The efficiency of fluorescence resonance energy transfer (E) was calculated from frequency modulated lifetime data using the following equation:

$$E = 1 - \tau_{da}/\tau_{d} \quad (1)$$

where τ_{da} is the lifetime of the fluorescence donor in the presence of an acceptor and τ_{d} is the lifetime in the absence of the acceptor. The distance between donor and acceptor probes was calculated from

$$R = R_0(E^{-1} - 1)^{1/6} \quad (2)$$

In this equation, R_0 is the Förster critical transfer distance (*32*) at which the energy transfer is 50% and is given by

$$R_0 = 9.79 \times 10^3(\kappa^2 n^{-4} Q_D J)^{1/6}\ (\text{Å}) \quad (3)$$

where κ^2 is the dipolar orientation factor, n is the refractive index of the medium taken as 1.4, a value that is typical for protein solutions (*33*), Q_D is the quantum yield of the donor and J is the overlap integral

$$J = \frac{\int_0^\infty F_D(\lambda)\epsilon_A(\lambda)\lambda^4\,d\lambda}{\int_0^\infty F_D(\lambda)\,d\lambda} \quad (4)$$

where $F_D(\lambda)$ is the fluorescence intensity of the donor at wavelength λ and $\epsilon_a(\lambda)$ is the molar absorbance of the acceptor at λ. The overlap integral was calculated by numerical integration. FRET distances were calculated with a Gaussian distribution around the mean value using the program CFS_LS,[2] which allows correction for incomplete acceptor labeling, as described in Lakowicz et al. (*34*). Due to inherent noise in the data, we have not been able to analyze the distance distribution, which was set at 5 Å for all measurements. Increasing the width of the distribution resulted in nonunique solutions.

Modeling. Since an atomic structure of the myosin head in the prepower stroke state containing the RLC and associated portion of the heavy chain was not available, we constructed a hybrid molecule: the catalytic domain and ELC from smooth muscle (*8*) and the RLC containing portion from skeletal S1 (*2*). The atomic model of a hybrid S1 was built using InsightII 98.0 (MSI, San Diego, CA), by first aligning common elements of the atomic structures (catalytic domain, ELC) followed by fusing the distal portion of the regulatory domain. The alignment was performed on residues 5−49 and 61−149 of the skeletal ELC and residues 789−812 of the skeletal heavy chain with the homologous residues 6−50 and 62−150 of the smooth S1 ELC and residues 798−821 of the smooth heavy chain (rms = 0.14 Å), using a program, SUPERCa, written in MATLAB v. 5 (The Math Works Inc., Natick, MA). The transformed coordinates of skeletal RLC and its associated HC coordinates were then used as the smooth RLC region coordinates. Homologous ELC region residues were determined by pairwise sequence alignment with the InsightII Homology module using the Dayhoff evolutionary scoring matrix (PAM250) (*36*), a gap penalty of 10, and a gap length penalty of 1.65.

Structural modeling of the domain rotations was performed using X-PLOR v. 3.1 (*35*). Briefly, a sphere of all possible positions of the terminal residue of the S1 heavy chain was generated by rotating the regulatory domain around three mutually orthogonal axes centered at a given residue. The extent of all rotations was random between 0 and 2π, and a typical run consisted of 20 000 rotations around each of the three axes. For each rotation, a table of distances between defined donor/acceptor sites (Cα positions) was constructed and filtered to select only those rotations that satisfied observed FRET/LRET distance changes. The coordinates of the lys843 Cα were then written as a pdb file to facilitate

[2] Available from the Center for Fluorescence Spectroscopy at http://charlie.ab.umd.edu/cfs/software/.

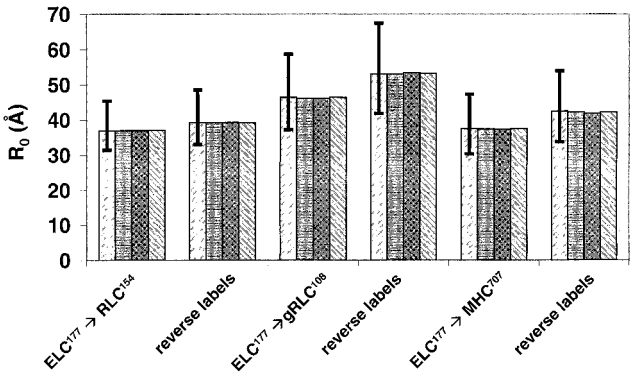

FIGURE 1: The Förster distance in various myosin states assuming $\kappa^2 = 2/3$. For each labeled site, from left to right: rigor; ADP, ATP, AlF_4^-. The error bar in rigor state denotes R_o calculated for maximum and minimum κ^2.

visualization of the allowed positions of the distal end of myosin head.

RESULTS

Fluorescence Parameters. The measured quantum yields (Q) of the AEDANS moiety on various sites were in general agreement with previously published data. For example the Q of AEDANS-ELC^{177} measured here was 0.29 as compared to 0.3 as measured by Marsh and Lowey (*17*), and for AEDANS-MHC^{707}, $Q = 0.50$ versus 0.48 for AEDANS-MHC^{707} as reported by the above authors. More importantly, we have found that the quantum yields, hence the overlap integrals, do not vary as a function of nucleotide state. Thus, the Förster distance does not change significantly in various myosin states, Figure 1, which allows us to interpret the changes in the transfer efficiency in terms of distance changes.

Another important fluorescence parameter affecting the efficiency of transfer is the orientation factor κ^2, which can take any value between 0 and 4 for static probe pairs. It is customary to assume a value of 2/3 for isotropic distribution of donor and acceptor transition dipole orientations, which results in a maximum error of approximately 20% in most cases (*37*). Probe mobility restricts the range of possible κ^2 values as the static distribution is partially averaged. The minimum and maximum κ^2 values are estimated from the depolarization of the fluorophore according to the formalism developed by Dale et al. (*38*).

$$\langle\kappa^2\rangle_{max} = \frac{2}{3}[1 + \langle d_D\rangle^{1/2} + \langle d_A\rangle^{1/2} + 3\langle d_D\rangle^{1/2}\langle d_A\rangle^{1/2}] \quad (5)$$

$$\langle\kappa^2\rangle_{min} = \frac{2}{3}[1 - 0.5\langle d_D\rangle^{1/2} - 0.5\langle d_A\rangle^{1/2}] \quad (6)$$

Depolarization values used in these equations can be obtained either from time-resolved fluorescence or from Perrin plots of steady-state fluorescence polarization $<d_A> = (r_o/r_f)$, where r_o and r_f are the initial and fundamental anisotropies of the donor and acceptor. Values for IAF and IAEDANS depolarization have been measured for many of the sites used here. The values were generally low for regulatory domain probes: 0.25 for AEDANS attached to ELC^{177}, 0.38 for RLC^{154}, with higher (0.66) values observed for MHC^{707} (*39*−*41*). The depolarization of DABMI, which is not fluorescent, was assumed to be that of the most rigid probe at a given site (the worst case scenario); for gRLC^{108} the depolarization value was assumed to be 0.7 as found for a rhodamine label attached to this site (*21*). These values, although not accurate, do not affect in any way our conclusions but they do provide informative error bars on the absolute values of distances measured (Figure 1). The minimum and maximum values for the Förster distance, R_o, corresponding to the extremes of κ^2 values are listed in Table 1.

Distances in Rigor: Comparison with Atomic Models. FRET is generally considered to be a low resolution structural technique sensitive mainly to changes in distances rather than to absolute distances. Even so, the comparison of crystallographic and FRET distances is favorable. In five of six cases, the measured value fell within 5 Å of the atomic model of chicken S1, Figure 2. This is very serendipitous considering the uncertainty in κ^2 and the finite size of the probes (∼15 Å), plus the flexible linker between protein and fluorophore, which allows some probes to sweep through a 15 Å diameter area on the surface of the protein (*42*).

Nevertheless, the agreement is good; for instance, the distance between RLC^{154} and ELC^{177} is 45.5 Å in the crystal structure, while we have measured the distance to be 43.1 Å in one direction and 42.3 Å when the donor and acceptor are reversed. The probe reversal helps to verify the assumptions made about κ^2 values. The $\kappa^2 = 2/3$ assumption should be an underestimate for one direction and an overestimate for the reverse direction resulting in lower and upper bounds for the actual distance. This is best illustrated for the distance between MHC^{707} of the catalytic domain and ELC^{177}. The distance calculated with $\kappa^2 = 2/3$ is 5 Å too long with the donor on ELC and 3 Å too short with the donor on MHC^{707} (Figure 2), while the average distance differs by only 1 Å from the atomic model. The gRLC^{108} to ELC^{177} distance deviates most from the atomic model, the crystal structure (*2*) places val103 (homologous to cys108 of gRLC) 33.3 Å away from ELC^{177} while the distance measured here is 31.6 Å in one direction and 43.2 Å in the other. However, even in the latter case, the crystal structure distance is within the distance calculated assuming a minimum value for κ^2.

Catalytic-Regulatory Domain Distances in Intermediate States. The distance changes between the catalytic domain and the ELC were measured in pre- and postpower stroke states. The postpower stroke states were induced by either the absence of any nucleotides or by the presence of MgADP. The prepower stroke states were achieved either in the presence of MgATP or MgADP/AlF_4^- (*43*). A small increase of distances (less than 1.2 Å) was observed in the nucleotide-bound states, Figure 3. However, we do not consider these changes to be significant. The experimental reproducibility of these changes (independent samples) is of a similar order, ±1 Å. Thus, if any changes actually occur between these sites, then the changes are less than 2 Å. In agreement with our finding for MHC^{707}, no significant distance changes were observed between two other sites on the catalytic domain (MHC^{83} and MHC^{553}) and ELC^{177} (*18*). Likewise, no change was observed for the MHC^{707} to gRLC^{108} distance (*19*).

Intradomain Distances: ELC−*RLC.* A similar absence of any significant changes between the pre- and postpower stroke states was obtained within the regulatory domain between ELC^{177} and the two RLC sites (RLC^{154} and gRLC^{108}). As illustrated in Figure 4 and Figure 5, there is

Table 1: Fluorescence Parameters of Donor/Acceptor Pairs

donor	site	acceptor	site	J (M^{-1} cm^3)	R_o(2/3) (Å)	R_o (min) (Å)	R_o(max) (Å)
IAEDANS	ELC^{177}	DABMI	RLC^{154}	5.9×10^{-14}	37.0	31.5	45.4
IAEDANS	RLC^{154}	DABMI	ELC^{177}	8.4×10^{-14}	39.3	33.1	48.6
IAEDANS	ELC^{177}	IAF	gRLC^{108}	2.2×10^{-13}	46.4	37.2	58.7
IAEDANS	gRLC^{108}	IAF	ELC^{177}	3.0×10^{-13}	53.0	41.8	67.5
IAEDANS	ELC^{177}	DABMI	MHC^{707}	6.2×10^{-14}	37.5	30.3	47.3
IAEDANS	MHC^{707}	IAF	ELC^{177}	2.9×10^{-13}	42.5	33.8	54.0

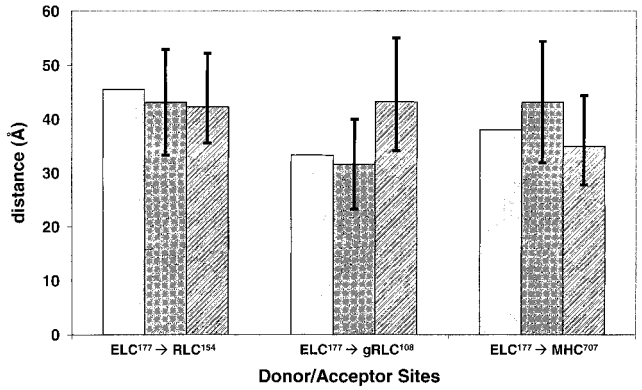

FIGURE 2: Comparison of FRET and crystallographic distances (between Cα) for ELC^{177} to RLC^{154} (left); ELC^{177} to gRLC^{108} (middle) and ELC^{177} to heavy chain MHC^{707} (SH1) (right). The left bar of each group represents the crystallographic value, the filled bar is for the values with the donor attached to ELC^{177} and the stippled bar is for the reverse direction. The error bars denote the distances calculated assuming minimum and maximum κ^2 values.

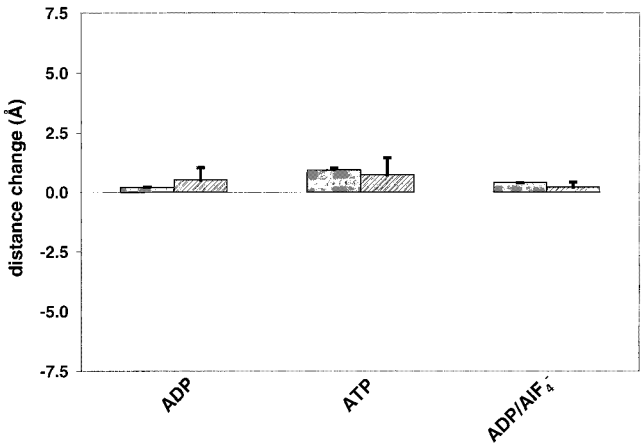

FIGURE 3: Distance changes between catalytic and regulatory domains in pre- and postpower stroke states. The difference between the rigor state and ADP (left), ATP (middle), and ADP/AlF_4^- (right). The solid bar denotes distance change measured with donor attached to ELC^{177}, stippled bar denotes distance change with donor on the cys707 of catalytic domain, MHC^{707}. The error bars denote the standard deviation of at least three independent protein preparations.

no change greater than 2 Å in any of the states. For ELC^{177}–RLC^{154}, the changes observed in one direction are reversed when the probes are reversed (Figure 4). Thus, these small <2 Å changes are most likely the result of changes in orientation of the dipole of the probe attached to RLC^{154} and not due to translational movement of the two sites. Molecular modeling of the RLC^{154} environment reveals the most severe steric restrictions and hence the highest sensitivity to reorientation of the four sites under study.

Figure 5 confirms the basic conclusion for the second more proximal site on the gRLC^{108}. Five out of six measured

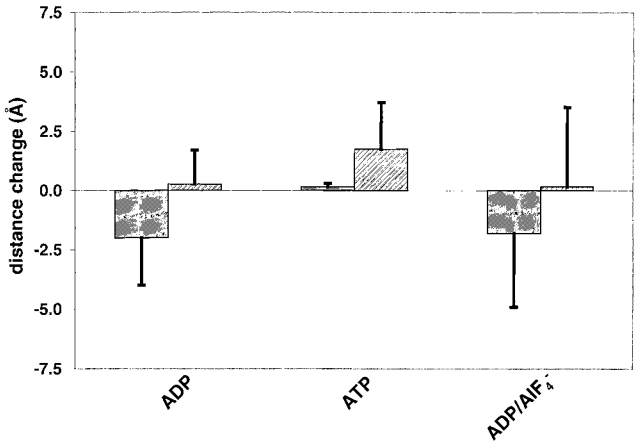

FIGURE 4: Segmental distance change within the regulatory domain. Intra-domain changes in the distance between ELC^{177} and RLC^{154} with respect to the rigor state were effected by addition of ADP (left), ATP (middle), and ADP/AlF_4^- (right). The solid bar denotes distance change measured with donor attached to ELC^{177}, stippled bar denotes distance change with donor on the RLC^{154}. The error bars denote the standard deviation of at least three independent protein preparations.

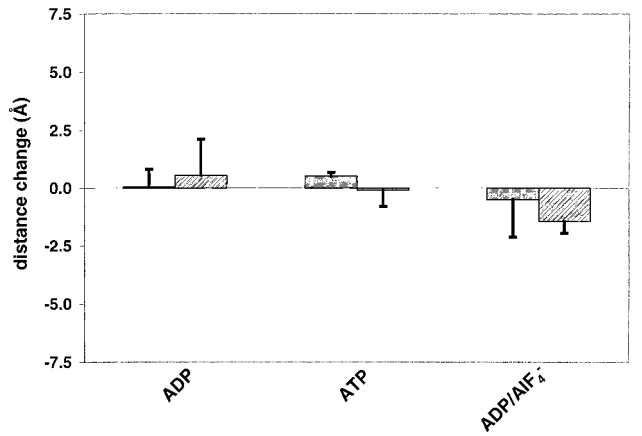

FIGURE 5: Segmental distance change within the regulatory domain. Intradomain changes in the distance between ELC^{177} and gRLC^{108} were effected by addition of ADP (left), ATP (middle), and ADP/AlF_4^- (right) *to rigor*. The solid bar denotes distance change measured with donor attached to ELC^{177}, stippled bar denotes distance change with donor on gRLC^{108}. The error bars denote the standard deviation of at least three independent protein preparations.

distances in various states do not change more than 0.5 Å, and the largest change is 1.4 Å (for the AlF_4^- state with the donor on gRLC). These changes are well within experimental error and we do not consider them to be significant.

Modeling. To interpret our observations in terms of a possible contribution of intradomain flexibility to the power stroke, we have determined all possible configurations of the regulatory domain constrained by observed FRET distance changes. The distal part of the regulatory domain (the RLC region) was randomly rotated 20 000 times as a

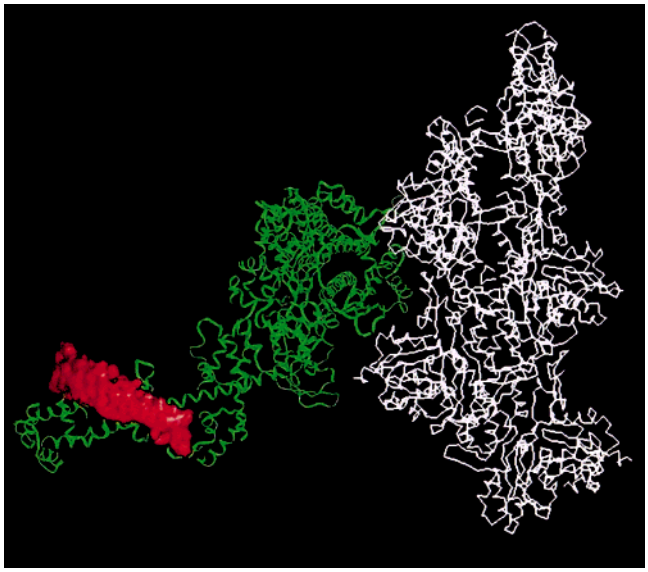

FIGURE 6: Model of actomyosin complex with the surface denoting the movement of the tail of the myosin head consistent with FRET results between ELC and RLC.

Table 2: Distance Restraints Used in Modeling of Changes between Pre- and Postpower Stroke States

sites	lower bound of the change[a]	upper bound of the change[a]	ref
MHC^{553}-ELC^{177}	−3.0	4.0	*18*
MHC^{131}-ELC^{177}	−8.0	−0.9	*18*
MHC^{707}-ELC^{177}	−1.0	2.2	this work
MHC^{131}-$RLC^{N-term.}$	−1.0	5.0	*20*
MHC^{131}-RLC^{108}	−5.6	−0.5	*21*

[a] Distance change in prepower stroke states (ATP, AlF_4^-, and BeF_x) is calculated with respect to rigor, or ADP states, the range of values was estimated from the scatter of the values in the pre- and postpower states ±1 Å.

rigid body about three mutually orthogonal axes centered at the ELC−RLC interface where the long α-helix of the heavy chain is most exposed. We have chosen glu802 as a pivot point, however, other residues in that region were also considered with no effect on the conclusions. To visualize the effect of these rotations, we have plotted the position of lys843 in the tail of the regulatory domain in Figure 6. The surface forming a narrow band is generated by the lys843 positions for rotations which changed the distance between ELC^{177}−RLC^{154} and $gRLC^{108}$ by less than 2 Å. Thus, this surface represents all possible excursions of the regulatory domain tail that are consistent with the observed FRET distance changes. Inspection of the *z*-coordinate of this surface establishes 22 Å as an upper bound for the potential contribution of intradomain changes to the power stroke.

A similar approach was taken in modeling the geometry of the regulatory domain with respect to the catalytic domain. In addition to FRET distance changes observed here, we have used published constraints between a number of sites within the myosin head, including LRET and FRET data, Table 2. As before, the distances between these sites were calculated for each random rotation, and the rotations satisfying observed restraints were selected. The position of lys843 is plotted in Figure 7 for the two published models of the myosin head. Rayment's structure of chicken S1 (2) was assumed to approximate the postpower stroke state, and Cohen's structure of smooth muscle S1 with $MgADP{\cdot}AlF_4^-$ (*8*) was assumed to be a model for a prepower stroke state, Figure 7.

The surface traced by the tail of the regulatory domain, consistent with all the measurements, has approximate dimensions of 134 Å × 39 Å along the filament axis and perpendicular to it, respectively, when using the chicken S1 structure as a final (postpower stroke) structure. Alternatively, when the Cohen structure is used in the modeling process as a prepower stroke structure, there are two allowed areas: one centered around the original Cohen prepower stroke structure and the second located toward the *z*-line, 125 Å along the actin filament axis in the direction of the predicted power stroke.

Qualitatively, the movement of the tail of the regulatory domain that is suggested by our modeling is consistent with that postulated from the atomic structures of the different myosin states: the down-swing from the bent prepower stroke state structure to the extended structure observed in the absence of nucleotides. The absence of an atomic structure in each of these two states from the same myosin isoform precludes a more quantitative analysis. It seems though that the Cohen and Rayment structures represent reasonable approximations of the pre- and postpower stroke structures, respectively, and that the LRET/FRET data when taken together are capable of detecting the movement of the regulatory domain that generates force, as postulated by Rayment (*2*). The extent of the power stroke as estimated from the overlap areas consistent with FRET/LRET results is 85 Å.

DISCUSSION

The measured distance between the catalytic domain and the proximal part of the regulatory domain, as well as the distance between the ELC and two sites on the RLC, agree well with the atomic model of the myosin head (*2*). The accuracy of our measurements was strengthened by determination of quantum yields in each state and by remeasuring these distances with the probes reversed, thus minimizing the effect of the orientation factor κ^2. Importantly, we have measured these inter- and intradomain distances as a function of nucleotide-bound state and determined that there was no significant change in the transfer efficiency for any of the probe pairs. Molecular modeling was used to interpret the observed changes in terms of their contribution to the power stroke. The portions of the myosin head on either side of a putative hinge were rotated as a rigid body within the constraints of observed changes. Such modeling was found to be consistent with a less than 22 Å distance change in the location of the tail of myosin contributed by reorientation between the ELC and RLC during the power stroke. A larger, 85 Å, distance change is allowed for the rotation of regulatory domain with respect to catalytic domain.

Relationship to Other Studies. The transient nature of the power stroke makes study of its intermediate states by steady-state techniques difficult. Various nucleotide analogues are used to trap states believed to correspond to specific intermediates of the MgATPase cycle. In this study, we chose to measure distance changes in response to the binding of ADP/AlF_4^- and ATP, thought to correspond to prepower stroke states (*43*). Electric birefringence and X-ray scattering

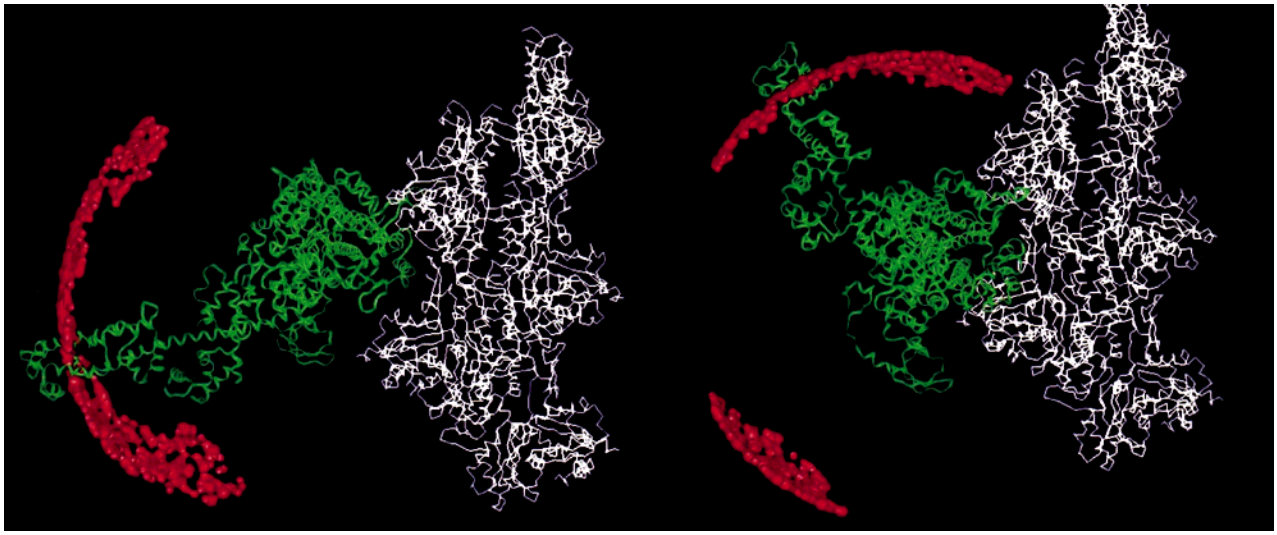

FIGURE 7: Movement of the tail of the myosin head consistent with FRET/LRET changes. Dark surfaces denote tail positions triangulated by the five distance measurements listed in (Table 2). (Left) FRET determined position of the regulatory domain in prepower stroke states assuming Rayment's model as a postpower stroke state; (Right) Position of the tail in postpower stroke states assuming Cohen's model as a prepower stroke state.

data indicate that the myosin head is more compact in these states as compared to the more elongated postpower stroke states induced by ADP or in the absence of nucleotide (*3, 44*).

Atomic resolution models of S1 provide support for the structure of these putative states (*1, 8*). There is a large, ~70° swing of the regulatory domain between nucleotide free skeletal S1 and smooth muscle S1 in ADP/AlF_4^-. This relative reorientation results in a significantly more "compact" S1 in the prepower stroke state, while the postpower stroke state is more elongated. However, care should be exercised in interpreting these structures; since the assignment of the nucleotide-free S1 to the postpower stroke state is not clear (Rayment, personal communication), the muscle isoforms are different in the two studies and any dynamic structural changes can be masked in the X-ray determined models. A complementary approach to crystallographic studies is to measure shape changes in solution by determining distances between selected sites within the myosin head. A number of groups have used FRET to search for these changes.

To list some of these: Marsh and Lowey (*17*) found a small change (~1 Å) in the relative positions of MHC^{707} (SH1) and ELC^{177} on addition of ATP, Takashi et al. (*45*) found a similarly small change between MHC^{707} and MHC^{83} (reactive lysine), and Moss and Trentham (*42*) have reported no change of the distance between the active site and ELC^{177} on hydrolysis of ATP. More recently, Smyczynski and Kasprzak (*18*) measured changes in a series of distances from ELC^{177} to MHC^{553} as well as ELC^{177} to the active site in pre- and postpower stroke states. As before, no significant changes were seen, prompting the authors to suggest that no bending occurs in the middle of the crossbridge.

The application of lanthanide-based luminescence resonance energy transfer (LRET), which has the advantage of longer distance sensitivity and fully depolarized donor emission, enabled measurements of the large distance between the catalytic domain and the distal portion of regulatory domain (RLC). Cooke, Selvin and co-workers observed a small, but statistically significant, 5 Å change in the distance between the active site and the $gRLC^{108}$, which was taken as evidence for a shape change accompanying the power stroke, consistent with the postpower stroke state being the more extended structure (*21*). Xu and Root (*20*), who measured a similar distance between the regulatory and catalytic domains (N-terminus of RLC to active site), interpret the distance changes they observed as placing a large constraint on the power stroke size; their results being inconsistent with the proposed powerstroke of 12 nm suggested by the swinging lever arm models of Rayment (1993) and Holmes (1997).

Our experiments extend the above structural and spectroscopic studies in two important ways. First, we measured the RLC to ELC distance and the ELC to catalytic domain distance separately in order to better define the proposed point of flexibility within S1. Second, we attempted to resolve the ambiguities in FRET and LRET measurements mentioned above by making multiple probe measurements, which included reversal of probe pairs, the use of multiple sites and the determination of R_o in each state.

With regard to the first point, Xiao et al. (*21*) localized the point of bending within the myosin head to a region between the RLC and the nucleotide site, encompassing approximately 50% of the length of the myosin head. We localize the bending of the head to the more discrete region between the MHC^{707} residue in the catalytic domain, and the ELC^{177}, approximately 20% of the length of S1. Our recent studies of domain dynamics have implicated this region as the flexible region in S1 (*14*).

With respect to the second point, several factors can alter the efficiency of energy transfer, in addition to a change in the distance separating the probes. These are quantum yield, spectral overlap, and orientation factor. A change in the quantum yield and a change in the spectral overlap of donor and acceptor emission and absorption bands, which occur due to changes in the microenvironment polarizability, all influence the Förster distance. In addition, the conformational changes often lead to a change in the relative orientation of the transition dipoles and thus changes of κ^2. In an effort to minimize these problems, we measured the quantum yield

of all donors at all sites as a function of bound nucleotide state, and we remeasured all distances with each probe pair reversed. We have considered variation in κ^2 based on published anisotropies at each site in an attempt to quantify maximum errors in distance changes. General agreement between our measured distances and the crystallographic structure justifies the above approach.

Intradomain Changes. The motivation for measuring the distance between the two light chains of myosin was to test whether the regulatory domain behaves as a passive, rigid lever or whether it changes its conformation in various myosin states. Highsmith and Eden (*6*) have recently noted a decrease of segmental flexibility in a complete myosin head with RLC present as compared to a shorter chymotryptic S1 containing only ELC. Our ST-EPR results comparing segmental mobility of ELC and RLC also point to a similar rate of motions in the regulatory domain (*46*). The presence of similar segmental mobility across the length of the regulatory domain does not preclude more static conformational changes between the two light chains. However, Figure 4 and Figure 5 clearly show that the distance between the ELC and RLC does not change significantly as a function of myosin state, implying that the domain is rigid and, thus, allowing it to act as a lever arm during force generation. While the rigid lever hypothesis is intuitively logical and generally accepted, the evidence is still the object of research. The strongest support comes from in vitro mobility studies, in which the translocation rate and power stroke distance increased with increasing length of the regulatory domain (*47*). However, this effect was somewhat smaller than that expected from an absolutely rigid lever. An increase in the number of myosin light chains in genetically engineered myosins resulted in smaller acceleration of the in vitro rate (*48*) than the substitution of the regulatory domain by rigid α-actinin fragments of similar lengths (*49*). More support for a flexible lever comes from a recent report (*50*) comparing the length of the power stroke between various myosin isoforms: myosin I containing six light chains; brush border myosin with three light chains, and smooth and skeletal myosin with two light chains. The size of the power stroke did not correlate with length of the regulatory domain, leaving open a possibility of intradomain flexibility, especially for longer regulatory domains.

Modeling of FRET Changes. As many investigators before us, we also found no significant change in the MHC^{707}–ELC^{177} distance in response to nucleotide binding. However, we do not believe that the absence of a significant distance change excludes a conformational rearrangement between the catalytic and regulatory domains. There is ample evidence that the regulatory domain moves with respect to the catalytic domain, including our protein dynamic data (*14*), EM (*9*, *10*), fluorescence anisotropy (*51*), and EPR (*52*), as well as the crystal structures (*1*, *8*). Thus, we hypothesize that there is almost certainly a change in the interdomain distance that we measured, but that this change is smaller than the error of our measurement. Additionally, a rotation of the regulatory domain that is symmetric about a vector normal to the actin axis might not result in a large distance change. The same problem has confounded other investigators (*18*, *20*). To obtain a global solution for putative motion of the regulatory domain with respect to the catalytic domain, we have modeled the distance constraints found here and by others (Table 2).

As the origin of rotations we have selected MHC^{770}, a site implicated by comparison of X-ray structures (*8*). To allow for all possible modes of reorientation including twisting, slew, and tilting, we have rotated the regulatory domain about three mutually orthogonal axes. Furthermore, in order not to bias our modeling toward any particular crystal structure, we have considered both the postpower stroke structure of skeletal S1 (*2*) and the prepower stroke structure created from smooth muscle (*8*). The most notable conclusion from modeling is that the distance changes that have been observed between the catalytic and regulatory domains are consistent with a power stroke, within the constraints of the surfaces shown in Figure 7. The upper bound for a power stroke consistent with the LRET/FRET results and the experimental errors in the literature is 85 Å when measured along the actin filament axes. This value is consistent with the current estimates of the 5−8 nm step size determined by laser-trap experiments (*53*−*55*).

Similar analysis of the ELC−RLC distances establishes a maximum contribution of the intradomain flexibility to the power stroke of 22 Å along the filament axes. Thus, if such a motion occurs it does not contribute more than a third of the total power stroke. It is important to realize that the precise choice of the pivot point location did not markedly alter the cone of swing generated by our modeling. Our conclusions for the pivot point being located at residue 796 were the same as for 802 of MHC.

In conclusion, we have found that the distances measured between catalytic and regulatory domains as well as the distances within the regulatory domain do not significantly change with the myosin ATPase state. Structural modeling suggests that the energy-transfer data are consistent with a power stroke distance of 85 Å due to flexing of the regulatory domain with respect to catalytic domain and establishes an upper bound of 22 Å for any contribution of RLC-ELC intradomain bending.

ACKNOWLEDGMENT

Dr. Doug Root is thanked for sharing with us the coordinates of the N-terminus of RLC and for critical reading of the manuscript and Dr. Ivan Rayment for providing us with the atomic coordinates of myosin head.

REFERENCES

1. Rayment, I., Holden, H. M., Whittaker, M., Yohn, C. B., Lorenz, M., Holmes, K. C., and Milligan, R. A. (1993) *Science 261*, 58−65.
2. Rayment, I., Rypniewski, W. R., Schmidt-Bäse, K., Smith, R., Tomchick, D. R., Benning, M. M., Winkelmann, D. A., Wesenberg, G., and Holden, H. M. (1993) *Science 261*, 50−8.
3. Highsmith, S., and Eden, D. (1990) *Biochemistry 29*, 4087−93.
4. Gollub, J., Cremo, C. R., and Cooke, R. (1999) *Biophys. J. 76*, A47.
5. Mendelson, R. A., Schneider, D. K., and Stone, D. B. (1996) *J. Mol. Biol. 256*, 1−7.
6. Eden, D., and Highsmith, S. (1997) *Biophys. J. 73*, 952−8.
7. Fisher, A. J., Smith, C. A., Thoden, J. B., Smith, R., Sutoh, K., Holden, H. M., and Rayment, I. (1995) *Biochemistry 34*, 8960−72.

8. Dominguez, R., Freyzon, Y., Trybus, K. M., and Cohen, C. (1998) *Cell 94*, 559−71.
9. Jontes, J. D., Wilson-Kubalek, E. M., and Milligan, R. A. (1995) *Nature 378*, 751−3.
10. Whittaker, M., Wilson-Kubalek, E. M., Smith, J. E., Faust, L., Milligan, R. A., and Sweeney, H. L. (1995) *Nature 378*, 748−51.
11. Fajer, P. G., Fajer, E. A., and Thomas, D. D. (1990) *Proc. Natl. Acad. Sci. U.S.A. 87*, 5538−42.
12. Ling, N., Shrimpton, C., Sleep, J., Kendrick-Jones, J., and Irving, M. (1996) *Biophys. J. 70*, 1836−46.
13. Baker, J. E., Brust-Mascher, I., Ramachandran, S., LaConte, L. E., and Thomas, D. D. (1998) *Proc. Natl. Acad. Sci. U.S.A. 95*, 2944−9.
14. Adhikari, B., Hideg, K., and Fajer, P. G. (1997) *Proc. Natl. Acad. Sci. U.S.A. 94*, 9643−7.
15. Botts, J., Takashi, R., Torgerson, P., Hozumi, T., Muhlrad, A., Mornet, D., and Morales, M. F. (1984) *Proc. Natl. Acad. Sci. U.S.A. 81*, 2060−4.
16. Botts, J., Thomason, J. F., and Morales, M. F. (1989) *Proc. Natl. Acad. Sci. U.S.A. 86*, 2204−8.
17. Marsh, D. J., and Lowey, S. (1980) *Biochemistry 19*, 774−84.
18. Smyczynski, C., and Kasprzak, A. A. (1997) *Biochemistry 36*, 13201−7.
19. Burmeister Getz, E., Cooke, R., and Selvin, P. R. (1998) *Biophys. J. 74*, 2451−8.
20. Xu, J., and Root, D. D. (1998) *J. Struct. Biol. 123*, 150−61.
21. Xiao, M., Li, H., Snyder, G. E., Cooke, R., Yount, R. G., and Selvin, P. R. (1998) *Proc. Natl. Acad. Sci. U.S.A. 95*, 15309−14.
22. Eads, T. M., Thomas, D. D., and Austin, R. H. (1984) *J. Mol. Biol. 179*, 55−81.
23. Wagner, P. D. (1982) *Methods Enzymol. 85*, 72−81.
24. Toste, A. P., and Cooke, R. (1979) *Anal. Biochem. 95*, 317−28.
25. Boey, W., Huang, W., Bennetts, B., Sparrow, J., Dos Remedios, C., and Hambly, B. (1994) *Eur. J. Biochem. 219*, 603−610.
26. Grand, R. J., and Perry, S. V. (1983) *Biochem. J. 211*, 267−72.
27. Kekic, M., Huang, W., Moens, P. D. J., Hambly, B. D., and dos Remedios, C. G. (1996) *Biophys. J. 71*, 40−7.
28. Wikman-Coffelt, J., Srivastava, S., and Mason, D. T. (1979) *Biochimie 61* (11−12), 1309−14.
29. Lanzetta, P. A., Alvarez, L. J., Reinach, P. S., and Candia, O. A. (1979) *Anal. Biochem. 100*, 95−7.
30. Scott, T. G., Spencer, R. D., Leonard, N. J., and Weber, G. (1970) *J. Am. Chem. Soc. 92*, 687−95.
31. Werber, M. M., Peyser, Y. M., and Muhlrad, A. (1992) *Biochemistry 31*, 7190−7.
32. Förster, T. (1948) *Ann. Phys. 2*, 55−75.
33. Fairclough, R. H., and Cantor, C. R. (1978) *Methods Enzymol. 48*, 347−79.
34. Lakowicz, J. R., Gryczynski, I., Wiczk, W., Kusba, J., and Johnson, M. L. (1991) *Anal. Biochem. 195*, 243−54.
35. Brunger, A. T. (1992) *X-PLOR: A system for X-ray crystallography and NMR*, Yale University Press, New Haven.
36. Dayhoff, M. O., Barker, W. C., and Hunt, L. T. (1983) *Methods Enzymol 91*, 524−45.
37. Stryer, L. (1978) *Annu. Rev. Biochem. 47*, 819−46.
38. Dale, R. E., Eisinger, J., and Blumberg, W. E. (1979) *Biophys. J. 26*, 161−93.
39. Wolff-Long, V. L., Tao, T., and Lowey, S. (1995) *J. Biol. Chem. 270*, 31111−8.
40. Trayer, H. R., and Trayer, I. P. (1988) *Biochemistry 27*, 5718−27.
41. Trayer, H. R., and Trayer, I. P. (1983) *Eur J Biochem 135*, 47−59.
42. Moss, D. J., and Trentham, D. R. (1983) *Biochemistry 22*, 5261−70.
43. Maruta, S., Henry, G. D., Sykes, B. D., and Ikebe, M. (1993) *J. Biol. Chem. 268*, 7093−100.
44. Wakabayashi, K., Tokunaga, M., Kohno, I., Sugimoto, Y., Hamanaka, T., Takezawa, Y., Wakabayashi, T., and Amemiya, Y. (1992) *Science 258*, 443−7.
45. Takashi, R., Muhlrad, A., and Botts, J. (1982) *Biochemistry 21*, 5661−8.
46. Baumann, B. A. J., Hambly, B., Hideg, K., and Fajer, P. G. (1999) *Biophys. J. 76*, A49.
47. Uyeda, T. Q., Abramson, P. D., and Spudich, J. A. (1996) *Proc. Natl. Acad. Sci. U.S.A. 93*, 4459−64.
48. Trybus, K. M., and Chatman, T. A. (1993) *J. Biol. Chem. 268*, 4412−9.
49. Anson, M., Geeves, M. A., Kurzawa, S. E., and Manstein, D. J. (1996) *EMBO J. 15*, 6069−74.
50. Veigel, C., Kendrick-Jones, J., Sellers, J. R., Sparrow, J. C., and Molloy, J. E. (1999) *Biophys. J. 76*, A145.
51. Hopkins, S. C., Sabido-David, C., Corrie, J. E., Irving, M., and Goldman, Y. E. (1998) *Biophys. J. 74*, 3093−110.
52. Hambly, B., Franks, K., and Cooke, R. (1991) *Biophys. J. 59*, 127−38.
53. Guilford, W. H., Dupuis, D. E., Kennedy, G., Wu, J., Patlak, J. B., and Warshaw, D. M. (1997) *Biophys. J. 72*, 1006−21.
54. Molloy, J. E., Burns, J. E., Kendrick-Jones, J., Tregear, R. T., and White, D. C. (1995) *Nature 378*, 209−12.
55. Finer, J. T., Simmons, R. M., and Spudich, J. A. (1994) *Nature 368*, 113−9.

BI991164Z